Inorganic Chemistry

Article

pubs.acs.org/IC

Electronic Spectra of *N*-Heterocyclic Pentacyanoferrate(II) Complexes in Different Solvents, Studied by Multiconfigurational Perturbation Theory

André Luiz Barboza Formiga,*[,†] Steven Vancoillie,[‡] and Kristine Pierloot*[,‡]

[†]Institute of Chemistry, University of Campinas−UNICAMP, P.O. Box 6154, 13083-970, Campinas, SP, Brazil

[‡]Department of Chemistry, University of Leuven, Celestijnenlaan 200F, B-3001 Heverlee, Belgium

ABSTRACT: Ligand-field and charge-transfer spectra of *N*-heterocyclic pentacyanoferrate(II) complexes $[Fe(CN)_5L]^{n-}$ were investigated using multiconfigurational perturbation theory. The spectrum of $[Fe(CN)_5(py)]^{3-}$ was studied in detail under vacuum and in the following polarizable continuum model (PCM) simulated solvents: acetone, acetonitrile, dimethylsulfoxide (DMSO), ethanol, methanol, and water. The ligand-field states proved to be rather insensitive to the solvent environment, whereas much stronger solvent effects were observed for the charge-transfer (CT) transitions. The nature of the intense band was confirmed as a metal-to-ligand charge transfer originating from a $3d_{xz} \rightarrow \pi^*_{b_1}$ (L)-orbital transition. The difference between the calculated and experimental transition energy of this CT transition is minimal for aprotic solvents, but increases strongly with the solvent proton donor ability in the protic solvents. In an attempt to improve the description of this CT state, up to 14 solvent molecules were explicitly included in the quantum model. In DMSO, the spectra of complexes with ligands L (where L is pyridine, 4-picoline, 4-acetylpyridine, 4-cyanopyridine, pyrazine, and *N*-methylpyrazinium) correlate very well with the experiment.

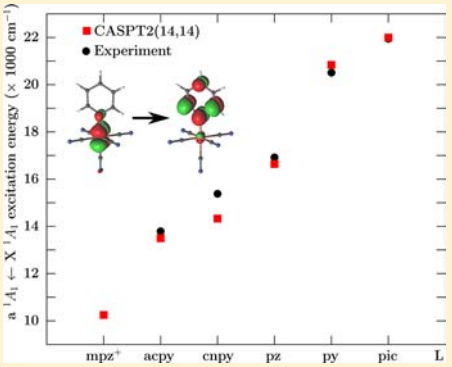

INTRODUCTION

During the last years, cyano-bridged molecular architectures have been extensively studied, because of their magnetic properties and the variety of structures that can be obtained, ranging from single-molecule magnets (SMM) to coordination polymers with different degrees of complexity.[1] Cyanide plays a special role as a bridge between two metal centers in this type of material, because of its ability to make strong covalent bonds with both metals, thus mediating exchange interactions. The interest in the synthesis of SMM based on the known Prussian Blue analogues has increased since high magnetic ordering temperatures were reported for compounds obtained from the $[Cr(CN)_6]^{3-}$ building block.[2]

Much attention has been given to the synthesis and structural properties of these materials, while spectroscopic studies are mainly focused on the metal-to-metal charge-transfer (MMCT) transitions, which is important in cases where photomagnetism is pursued.[3,4] However, there is an increasing number of examples where such compounds incorporate N-heterocyclic ligands in their structures and in such cases metal-to-ligand charge transfers (MLCTs) and ligand-to-metal charge transfers (LMCTs) can also be observed.[1]

The chemistry of mononuclear complexes of formulas $[Fe(CN)_5L]^{n-}$ in which L is an *N*-heterocyclic ligand was a main topic between 1970 and 1990, including the spectroscopic characterization of their charge-transfer (CT) spectra.[5] Ligand-field (LF) transitions are rarely observed, and the spectra show only one CT band and other transitions that can be associated to the ligands.[5] The assignment of the bands was made based on the experimental observation that CT bands are dependent on the solvent polarity. Qualitative descriptions of the bonding were used to interpret the effect of the nature of the ligand on the spectra and other properties. Apart from some studies focusing on cyanide-related CT spectra,[6] no theoretical investigations have appeared on MLCT spectra related to *N*-heterocycles. Very recently, Ene et al. reported density functional theory (DFT) and time-dependent density functional theory (TDDFT) studies on pentacyanoferrate(III) complexes coordinated to pyrazine and 4,4′-bipyridine and their corresponding LMCT spectra.[7]

In this article, we report on the study of the electronic structure and spectra of compounds with the general formula $[Fe(CN)_5L]^{n-}$ in which L is an *N*-heterocyclic ligand, as shown in Figure 1. All complexes are low-spin d^6, i.e., of the five (predominantly) Fe 3*d* orbitals, three $3d_\pi$ (corresponding to t_{2g} in octahedral symmetry) are occupied in the ground state, whereas two $3d_\sigma$ orbitals (corresponding to e_g in O_h) are empty. The UV−vis region of the spectrum should therefore consist of $3d_\pi \rightarrow 3d_\sigma$ LF transitions, while the presence of the N-heterocyclic ligand L is expected to give rise to low-lying $3d_\pi \rightarrow L\pi^*$ MLCT excitations. Both types of transitions were investigated in detail, making use of multiconfigurational perturbation theory based on a complete-active-space self-

Received: July 3, 2013
Published: August 30, 2013

   dx.doi.org/10.1021/ic401704r | *Inorg. Chem.* 2013, 52, 10653−10663

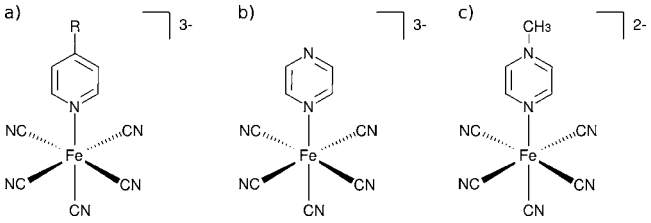

Figure 1. Coordination compounds investigated in this article, $[Fe(CN)_5L]^{n-}$, where (a) L = pyridine and derivatives (R= H (py), CH_3 (pic), CN (cnpy), C═O(CH_3) (acpy)), (b) L = pyrazine (pz), and (c) L = *N*-methylpyrazinium (mpz^+).

consistent field (CASSCF) reference wave function (i.e., the CASPT2 method). This method is particularly well-suited for the calculation of electronically excited states,[8−11] in particular for transition-metal complexes, for which the more popular TDDFT method is well-known to be afflicted with problems related to the optimal functional choice and the description of CT states.[10,11] The calculated spectra are compared to experimental data obtained in solution, and particular attention is given to the inclusion of solvent effects in the calculations by means of either a polarizable continuum model, or by explicitly including up to 14 solvent (water) molecules in the quantum chemical description.

COMPUTATIONAL DETAILS

As experimental data for distances and bond angles are lacking, ground-state geometries of the complexes were obtained from DFT calculations, making use of the B3LYP[12] and PBE0[13] hybrid functionals, and using def2-QZVPP basis sets for the Fe atom and def2-TZVP basis sets for all other atoms,[14] as defined in the Turbomole 6.4 program.[15] Implicit solvation effects were investigated in these DFT calculations by making use of the standard COSMO model,[16] as implemented in Turbomole. These calculations were performed with different dielectric constant values, thus modeling the following solvents: water (ε = 78.39), methanol (ε = 32.63), ethanol (ε = 24.55), dimethylsulfoxide (DMSO) (ε = 46.70), acetonitrile (ε = 36.64), and acetone (ε = 20.70), using the (nonoptimized) bond radii multiplied by 1.17, and all other settings set as the defaults in Turbomole 6.4. To improve the description of H-bonding by the protic solvents methanol, ethanol, and water, additional calculations were performed for $[Fe(CN)_5(py)]^{3-}$ in which several solvent molecules (i.e., five for all three solvents, fourteen for water) were treated explicitly in the quantum model, still using COSMO to treat implicit solvation of these supramolecular aggregates. All geometries were optimized without any symmetry constraints. However, apart from the clusters with explicit solvent molecules, the resulting structures all showed at least C_s (L = pic, acpy, mpz^+) or C_{2v} symmetry (L = py, cnpy, pz). Vibrational frequency analyses were performed to confirm that these symmetric structures indeed correspond to minima on the potential energy surface.

Multiconfigurational calculations were performed for spin-allowed ligand-field (LF) and charge-transfer (CT) excitations, using the implementation of CASSCF and CASPT2 in Molcas 7.6.[17,18] Single-point CASPT2 calculations were performed using the structures obtained from PBE0. ANO-RCC type basis sets[19] were used, and the influence of the size of the basis set on the excitation energies was investigated by using three different contraction schemes (see Table 1). The Cholesky decomposition technique was used to approximate the two-electron integrals, using an approximation threshold of 10^{-6} a.u.[20,21]

All CASSCF/CASPT2 calculations were performed making use of the full symmetry of the complexes. The choice of coordinates puts the organic ligand in the *yz*-plane and the CN^- group *trans* to it, lying on the *z*-axis. As a consequence, the $[Fe(CN)_4]$ plane corresponds to *xy*, with the CN^- ligands between the *x*- and *y*-axes. The CASSCF active space was chosen to include 14 electrons in 14 orbitals, denoted as CAS(14,14), and consisting of the five 3*d* orbitals, their cyanide counterparts of the same symmetry (i.e., two CN σ and three CN π^* orbitals (although the latter three are heavily mixed with Fe 4*d* character)), and the two highest π and two lowest π^* orbitals of the *N*-heterocyclic ligand L. All considered organic ligands are six-membered rings, and they all possess three empty π^* orbitals, $2b_1 + a_2$ in C_{2v}, that might be involved in MLCT transitions. However, preliminary CASSCF calculations (on $[Fe(CN)_5(py)]^{3-}$) including all three π^* orbitals showed that excitations into the second π^* orbital of b_1 symmetry are high-lying (at 60 000 cm^{-1}, i.e., in the UV region). Therefore, this π^* orbital was not included in the active space. A plot of the 14 (ground-state) active orbitals of $[Fe(CN)_5(py)]^{3-}$ is provided in Figure 2, and their composition, energy, and occupation number are given in Table 2.

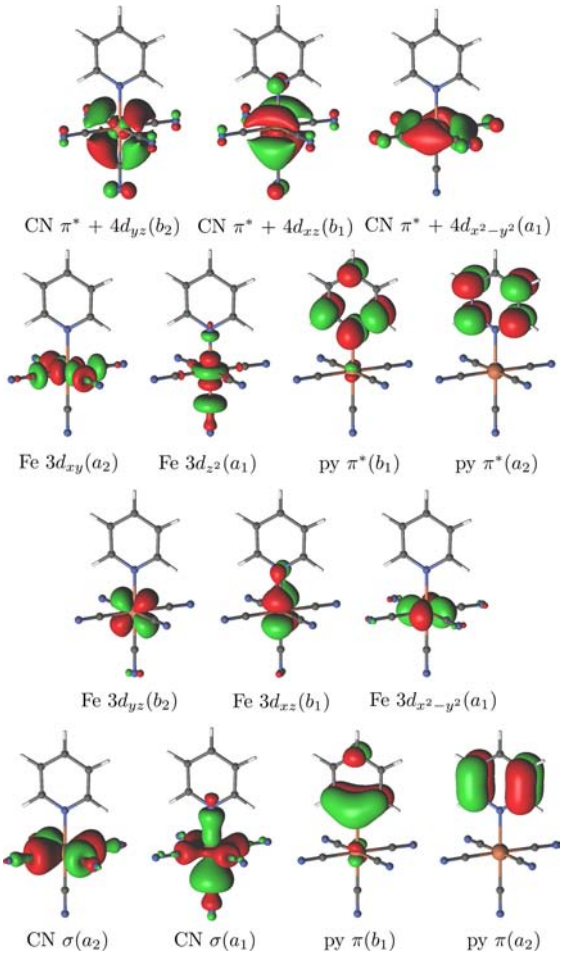

Figure 2. Active molecular orbitals of $[Fe(CN)_5(py)]^{3-}$.

Table 1. Basis Set Primitives and Contractions Used in the CASSCF/CASPT2 Calculations

basis set	Fe	C, N, O	H
bs1	(21s15p10d6f)/[5s4p3d1f]	(14s9p4d)/[3s2p1d]	(8s4p)/[2s1p]
bs2	(21s15p10d6f4g)/[7s6p5d2f1g]	(14s9p4d)/[4s3p1d]	(8s4p)/[2s1p]
bs3	(21s15p10d6f4g2h)/[7s6p5d3f2g1h]	(14s9p4d3f)/[4s3p2d1f]	(8s4p)/[3s1p]

dx.doi.org/10.1021/ic401704r | *Inorg. Chem.* 2013, 52, 10653−10663

Table 2. Active Molecular Orbitals of $[Fe(CN)_5(py)]^{3-}$, Obtained from a Ground-State CAS(14,14) Calculation in Water

orbital	energy[a] (a.u.)	occupancy number[b]	Composition (%)[c] Fe	CN	py
CN $\sigma(a_1)$	−0.470	1.974	31	61	8
CN $\sigma(a_2)$	−0.464	1.972	35	65	0
py $\pi(b_1)$	−0.450	1.930	5	0	95
py $\pi(a_2)$	−0.339	1.940	0	0	100
Fe $3d_{yz}(b_2)$	−0.385	1.956	93	7	0
Fe $3d_{xz}(b_1)$	−0.371	1.956	88	7	5
Fe $3d_{x^2-y^2}(a_1)$	−0.372	1.953	91	9	0
py $\pi^*(b_1)$	0.195	0.074	5	0	95
py $\pi^*(a_2)$	0.166	0.060	0	0	100
Fe $3d_{xy}(a_2)$	0.450	0.039	80	20	0
Fe $3d_{z^2}(a_1)$	0.454	0.036	82	16	2
CN π^* + Fe $4d_{x^2-y^2}(a_1)$	0.671	0.041	70	30	0
CN π^* + Fe $4d_{yz}(b_2)$	0.739	0.037	73	27	0
CN π^* + Fe $4d_{xz}(b_1)$	0.749	0.035	69	26	5

[a]Corresponding to the canonical orbitals. [b]Corresponding to the natural orbitals. [c]Based on Mulliken population analysis of the natural orbitals.

For comparison, the LF excited states of $[Fe(CN)_5(py)]^{3-}$ were also calculated with a reduced active space of only 10 orbitals, CAS(10,10) (i.e., not including the L(π,π^*) orbitals). Such a 10-orbital active space has been shown to provide an accurate CASPT2 description of the LF spectra of hexacyanometalate complexes.[22] However, we suspect that the presence of low-lying MLCT transitions to the π^* orbitals of the *N*-heterocyclic ligand might deteriorate the CASPT2 results for the LF excitation energies, when based on an active space that does not include these π^* orbitals.

For the description of the CT excitations into the L ($\pi^*_{b_1}$, $\pi^*_{a_2}$) orbitals, including these two orbitals in the active space is, of course, indispensable. However, our experience from previous studies[23−25] is that extending the active space with extra ligand π-type orbitals may significantly improve the accuracy of CASPT2 or RASPT2 calculations involving the transfer of an electron into/out of the ligand π-system. By also including the two bonding L π-orbitals in the CAS(14,14) space, we aim to obtain CASPT2 results that are accurate to within 1000 cm^{-1} (i.e., similar as in previous benchmark calculations[23]) for all electronic transitions considered in this work.

Part of the results in this work were obtained using CASSCF orbitals that were optimized for an average of two states with the same iron oxidation state and the same symmetry (cf. Tables 4 and 6, presented later in this paper). Averaging over two states with a different Fe oxidation state was avoided in all cases but one, as this may be expected to deteriorate the CASPT2 results (because they would be based on an average of thoroughly different shaped orbitals, especially in the Fe 3*d* part, and, as such, far from optimal for either of the states).[26,27] The single exception concerns the A^1A_2 LF excited state of the complex $[Fe(CN)_5(mpz)]^{2-}$, which is quite strongly mixed with CT character (see further discussion and Table 5), giving rise to convergence problems in an individual orbital optimization. The energy reported for this state is therefore based on average orbitals for the A^1A_2 and the interfering (b^1A_2) CT state.

For the calculation of the oscillator strengths, the excitation energies obtained from CASPT2 were used, while the transition dipole moments were obtained from the corresponding CASSCF wave functions/orbitals, making use of the CAS state interaction method.[28] The transition between the ground state and the charge-transfer state of the same symmetry ($^1A_1$, giving rise to the intense CT band in the spectrum) was treated differently, in that, here, the orbitals used for calculating the transition dipole moment were obtained from state-averaged CASSCF calculations over the two states involved, rather than from individually optimized orbitals. The reason for doing so is that, when described with their own orbitals, these two states become strongly nonorthogonal, making the results from the CAS state interaction analysis less trustworthy.

In the CASSCF/CASPT2 calculations, solvation effects were included by making use of the polarizable continuum model (PCM) method[29] with default parameters. For the excited states, only the fast component of the reaction field was calculated for each individual state, while the slow component was taken from the ground state. In the CASPT2 calculations and the calculations of the transition dipole moments (RASSI), the reaction field effects to the one-electron Hamiltonian were added as a constant perturbation.

RESULTS AND DISCUSSION

Geometry of $[Fe(CN)_5(py)]^{3-}$. Because the geometries of the complexes have never been obtained experimentally, we started by investigating the structure of $[Fe(CN)_5(py)]^{3-}$ with two different DFT functionals. For comparison, the structure of $[Fe(CN)_6]^{4-}$ was also calculated. The effect of solvation was included by means of the COSMO model and the results are presented in Table 3. We have found that a staggered conformation of the pyridine ring, with respect to the $Fe(CN)_4$ plane, is always more stable than an eclipsed conformation.

Table 3. Influence of the DFT Functional and Solvation on the Distances and Angles in $[Fe(CN)_6]^{4-}$ and $[Fe(CN)_5(py)]^{3-}$

	functional	Value vacuum	water	DMSO	acetone
$[Fe(CN)_6]^{4-}$					
Fe−CN	B3LYP	2.029 Å	1.948 Å	1.950 Å	1.952 Å
	PBE0	1.985 Å	1.916 Å	1.916 Å	1.919 Å
C≡N	B3LYP	1.176 Å	1.171 Å	1.171 Å	1.171 Å
	PBE0	1.175 Å	1.170 Å	1.170 Å	1.170 Å
$[Fe(CN)_5(py)]^{3-}$					
Fe−CN, *trans*[a]	B3LYP	1.977	1.922 Å	1.922 Å	1.925 Å
	PBE0	1.949 Å	1.892 Å	1.893 Å	1.896 Å
Fe−CN, *cis*[a]	B3LYP	2.006 Å	1.956 Å	1.957 Å	1.959 Å
	PBE0	1.971 Å	1.926 Å	1.926 Å	1.928 Å
C≡N, *trans*	B3LYP	1.168 Å	1.169 Å	1.169 Å	1.169 Å
	PBE0	1.168 Å	1.169 Å	1.169 Å	1.169 Å
C≡N, *cis*	B3LYP	1.169 Å	1.168 Å	1.168 Å	1.169 Å
	PBE0	1.169 Å	1.168 Å	1.168 Å	1.168 Å
Fe−N(py)	B3LYP	2.029 Å	2.112 Å	2.112 Å	2.109 Å
	PBE0	1.987 Å	2.063 Å	2.061 Å	2.059 Å
Fe−C−N, *cis*	B3LYP	174.63°	179.05°	179.19°	179.61°
	PBE0	175.10°	179.27°	179.34°	179.69°
C−Fe−C	B3LYP	177.29°	179.41°	179.55°	179.89°
	PBE0	177.68°	179.07°	179.83°	179.87°

[a]Designations *trans* and *cis* correspond to pyridine.

Solvent effects were investigated in water, DMSO, and acetone, thus covering a wide range of dielectric constants (78.39, 46.70, and 20.70, respectively). What can be concluded is that the COSMO model does not provide significantly different structures for the various dielectric constants. However, considerable differences are found between the bond distances calculated under vacuum and in a solvent. The presence of the solvent medium provides an average reduction of 0.05 Å for the Fe−CN distance and an average increase of 0.07 Å for the Fe−N(py) bond distance. Another important solvent effect can be observed in the Fe−C−N bond angles for

dx.doi.org/10.1021/ic401704r | *Inorg. Chem.* 2013, 52, 10653−10663

Table 4. Ligand-Field Spectrum of $[Fe(CN)_5(py)]^{3-}$ under Vacuum and in Water, Calculated with CASPT2

		CASPT2 Excitation Energy (cm^{-1})					oscillator strength
		CAS(10,10)		CAS(14,14)			CAS(14,14)
state	principal excitation[a]	vacuum[b] bs2	water bs2	water bs1	water bs2	water bs3	water bs2
A^1B_2	$d_{yz} \rightarrow d_{z^2}$	23 341	24 091	24 169	24 069	23 596	1.9×10^{-3}
A^1B_1	$d_{xz} \rightarrow d_{z^2}$	24 475	24 246	24 227	24 172	23 745	2.2×10^{-3}
A^1A_2	$d_{x^2-y^2} \rightarrow d_{xy}$	29 748	29 813	29 293	29 255	29 270	0.0
A^1A_1	$d_{x^2-y^2} \rightarrow d_{z^2}$	28 146	29 874	30 271	29 862	29 863	6.8×10^{-5}
B^1B_2	$d_{xz} \rightarrow d_{xy}$	35 339	34 537	31 438	32 219	31 940	3.7×10^{-4}
B^1B_1	$d_{yz} \rightarrow d_{xy}$	35 021	34 693	32 995	33 010	32 847	7.3×10^{-4}

[a]The ground-state configuration is X^1A_1, with configuration $(d_{xz})^2(d_{yz})^2(d_{x^2-y^2})^2(d_{xy})^0(d_{z^2})^0$. [b]At ground-state geometry obtained in water.

the cyanides *cis* to pyridine. Bending of the Fe−C−N angles toward the pyridine ligand is observed under vacuum, whereas in a solvent surrounding the $[Fe(CN)_4]$ fragment is closer to planar.

If we compare the calculated results with the experimental crystal structure of the $[Fe(CN)_6]^{4-}$ complex (d_{Fe-CN} = 1.91−1.93 Å, d_{C-N} = 1.17 Å, averages),[30] we note that the PBE0 functional more closely reproduces the bond distances, giving smaller bond distances than B3LYP in all cases. As was investigated in ref 22, small changes in the ground-state Fe−CN distance may induce remarkable differences in the (vertical) position of electronically excited states. From Table 3, it is clear that the inclusion of solvent effects is necessary to obtain reasonable ground-state geometries.

Ligand-Field Spectra. The electronic spectra of *N*-heterocyclic pentacyanoferrate(II) complexes are dominated by a CT band that usually masks the ligand-field transitions.[31−33] Therefore, quantum chemical calculations may be very useful for obtaining information concerning the position of these ligand-field transitions, provided that a sufficiently high accuracy can be obtained from such methods. In this work, we make use of the CASPT2 method, a well-established method for the calculation of electronic spectra of both organic molecules and transition-metal complexes,[8] and even the spectra of heavy-metal complexes such as uranyl.[34] One of the first applications of the CASPT2 method in transition-metal chemistry, now more than 20 years ago,[22] concerned a systematic investigation of the ligand-field spectra of hexacyanometalate complexes, $M(CN)_6^{3-/4-}$ (M = V, Cr, Mn, Fe, Co), which are experimentally well-known.[35] Even though these calculations were performed with rather limited basis sets and not considering any influence from a surrounding crystal or solvent, the excitation energies obtained from CASPT2 were generally in reasonable agreement (i.e., within 3000 cm^{-1}) with the available experimental data. One of the goals of the present study is to estimate the accuracy that may be expected from the CASPT2 method in predicting the ligand-field (this section) and CT (next section) excitation energies in the electronic spectra of the considered pentacyanoferrate(II) complexes. These spectra are inherently more complicated than those for the parent hexacyano complexes, because the presence of the sixth *N*-heterocyclic ligand gives rise to the occurrence of CT transitions in the visible region of the spectrum, which, in the case of the hexacyano complexes, is preserved for the LF transitions.

Ligand-Field Spectrum of $[Fe(CN)_5(py)]^{3-}$. To start with, a systematic series of test calculations has been performed for the $[Fe(CN)_5(py)]^{3-}$ complex, using different basis sets, active spaces, and either including solvent effects or not. The results of these test calculations are shown in Table 4. The complex has C_{2v} symmetry, and the choice of axes leads to a $^1A_1$ ground state with principal configuration $(d_{xz})^2(d_{yz})^2(d_{x^2-y^2})^2(d_{xy})^0(d_{z^2})^0$. For a more-detailed description of the orbitals involved, we refer to Figure 2 and Table 2. From the closed-shell $^1A_1$ ground state, we expect six spin-allowed LF transitions, corresponding to the two 3-fold degenerate LF excited states $^1T_{1g}$, $^1T_{2g}$ in an octahedral d^6 complex. In C_{2v} symmetry, $^1T_{1g}$ reduces to $^1A_2 \oplus {}^1B_1 \oplus {}^1B_2$ and $^1T_{2g}$ reduces to $^1A_1 \oplus {}^1B_1 \oplus {}^1B_2$. These six singlet excited states were included in our calculations. They are labeled by capital letters in order to distinguish them from CT states of the same symmetry, which we will label with lower case letters (see the next section).

First, we look at both sets of CASPT2(10,10) calculations, performed with basis set 2 but either under vacuum or in water. Even though the complexes considered are highly negatively charged, we find that solvent effects are rather modest for the LF states and that there is no systematic trend. The largest effect is found for the A^1A_1 state, the energy of which is raised by 1700 cm^{-1} by the water environment. The A^1B_2 state is destabilized by 700 cm^{-1}, with respect to the ground state, while the B^1B_2 state is stabilized by the same amount. The other three states—A^1B_1, B^1B_1, and A^1A_2—remain virtually unaffected. The rather modest solvent effect for the LF transitions may be explained by the fact that these transitions essentially occur within the Fe 3*d* shell (cf. Table 2). As such, the solvent may be expected to have a similar stabilizing effect on the ground state and LF excited states. We can extend the results for $[Fe(CN)_5(py)]^{3-}$ to infer that the dielectric constant effect will not considerably affect the position of LF transitions in the other complexes either.

Second, the effect of the active space is investigated by comparing the results obtained with the CAS(14,14) active space to a smaller CAS(10,10) space in which the py (π,π^*) orbitals were not included. Both sets of calculations were performed with basis set 2 and in water. The 10 orbitals included in the CAS(10,10) space still suffice to describe all covalent iron−ligand interactions (and the static correlation effects connected to this type of interaction). Indeed, as one can see from the shape and composition of the active orbitals in Figure 2 and Table 2, the py (π,π^*) orbitals are hardly involved in covalent interactions with the metal. They remain almost completely localized on the py ligand, containing, at most, 5% Fe 3d character. As such, the presence of these orbitals in the active space might be expected to leave the LF transitions invariant, because those are essentially metal-centered. As Table 4 shows, this expectation is corroborated for the states A^1B_1, A^1B_2, and A^1A_1, which have an electron excited into Fe $3d_{z^2}$. The other three states—A^1A_2, B^1B_1, and B^1B_2, with $3d_{xy}$ singly

dx.doi.org/10.1021/ic401704r | Inorg. Chem. 2013, 52, 10653−10663

occupied—are lowered in energy in the CASPT2(14,14), compared to CASPT2(10,10), by 550−2300 cm^{-1}. This is caused by subtle mixing effects between the $3d_{xy}$ and the py π^*-orbitals of the same (a_2) symmetry. As we shall see in the next section (cf. Table 6), CT transitions to the py $\pi^*_{a_2}$-orbital occur at ∼27 000 cm^{-1} in water (i.e., at lower energies than the LF excitations into $3d_{xy}(a_2)$). Ignoring the interaction between the ($d_\pi \rightarrow d_{xy}$) LF and ($d_\pi \rightarrow$ py $\pi^*_{a_2}$) CT transitions in the CASSCF reference wave function (by excluding $\pi^*_{a_2}$ from the CAS(10,10) active space) results in a less-accurate treatment of this interaction in the perturbational step. Therefore, the CASPT2(14,14) calculations should be considered superior, and such calculations have also been performed for the LF spectra of the series of $[Fe(CN)_5L]^{n-}$ complexes with other *N*-heterocyclic L (see Figure 1). These results will be discussed further.

Third, the quality of the basis set was evaluated by calculating the same excitations in water using three basis sets (bs1−bs3). The most significant changes are observed for the three higher-lying states. The largest difference is −781 cm^{-1} (B^1B_1), when the basis quality is increased from bs1 to bs2. A further improvement of the basis (bs2 → bs3) does not lead to significant differences. As such, these results suggest that bs2 is sufficient to obtain accurate relative energies for the LF states.

All further discussion of the LF states below will be based on CASPT2(14,14) results with bs2 in water. This method was also used to obtain oscillator strengths. The analysis of the oscillator strengths and the energetic profile is consistent with the experimental evidence that the LF states cannot be observed in the ultraviolet−visible (UV-vis) spectra of $[Fe(CN)_5(py)]^{3-}$.[32] According to our results, only two transitions ($A^1B_1 \leftarrow X\ ^1A_1$ and $A^1B_2 \leftarrow X^1A_1$) are likely to be intense enough to be observed. However, their energy is quite similar to the energy observed for the intense CT band in the spectrum of this complex (27 320 cm^{-1} in water; see the next section). As a consequence, they are masked by this highly intense band.[36] The other transitions either have very low oscillator strengths, or are symmetry-forbidden (A^1A_2).

Ligand-Field Analysis. For a very long time, the theoretical description of the electronic structure and ligand-field spectra of transition-metal complexes has been the exclusive domain of ligand-field theory.[37,38] Moreover, today, the concepts of ligand-field theory are still extremely valuable for the interpretation of spectroscopic data obtained from highly accurate but much more complex MO methods, such as the multiconfigurational CASPT2 method used in this work. A formulation of ligand-field theory that has proven to be particularly successful is the angular overlap model (AOM).[39] In this model, destabilization and splitting of the metal *d*-orbitals in a ligand coordination environment are described as a superposition of contributions from individual metal−ligand pairs, which are independent of the other ligands and therefore, in theory, transferable between different complexes of the same metal ion. Each metal−ligand pair is described in terms of only two parameters: e_σ, e_π. In an octahedral complex MX_6, the contributions of the six ligands add up to produce a splitting of the *d*-orbitals equal to $\Delta_{oct}(X) = 3e_\sigma(X) - 4e_\pi(X)$ (i.e., the ligand-field strength of ligand X when bound to metal M). Based on experimental ligand-field spectroscopic data, a two-dimensional *spectrochemical series* has been constructed, ordering, respectively, series of ligands/metals with respect to the strength of the ligand field that they are producing when combined with the same metal/ligand. Repulsion between the metal *d*-electrons is in the AOM described by the so-called Racah parameters *A*, *B*, and *C*, which are reduced, compared to their value in the free metal ion, as the result of delocalization of the *d*-electrons over covalent M−X bonds. Also here, a classification of the tendency of different metals/ligands to form covalent bonds has been proposed in terms of the *nephelauxetic series*. Together, the ligand-field concepts of strong or weak σ-donation, π-donation or π-backdonation (manifested by a negative e_π), as well the description of covalency of metal−ligand bonds in terms of delocalization of the electrons originating from the metal *d*-shell, have formed, over the years, a common chemical language to describe the bonding and electronic structure of coordination complexes,[40,41] even if the concrete numbers behind the different ligand-field parameters are not always explicitly used. Many computational studies have also been reported over the years in which the results obtained from more-elaborate quantum chemical methods (wave function or DFT) were mapped to the AOM parametrization scheme, thus building a more direct bridge between ligand-field theory and more rigorous quantum chemical methods and giving access to (often unknown) AOM parameters from first principles theory.[42−46] Furthermore, it should also be noted that the AOM itself has recently been brought back to life in the ligand-field molecular mechanics (LFMM) theory of R. Deeth,[47,48] where it is used to offer a simple set of parameters to describe specific M−X force fields.

In an octahedral MX_6 d^6 complex, the energies of the two singlet LF excited states $^1T_{1g}$, $^1T_{2g}$, with respect to the $^1A_{1g}$ ground state, may be expressed in terms of the AOM parameters $e_\sigma(X)$, $e_\pi(X)$, and Racah parameters *B* and *C*, as follows:

$$E_{(^1T_{1g} \leftarrow {}^1A_{1g})} = \Delta_{oct}(X) - C \tag{1}$$

$$E_{(^1T_{2g} \leftarrow {}^1A_{1g})} = \Delta_{oct}(X) + 16B - C \tag{2}$$

In a substituted complex MX_5L, the two states $^1T_{1g}$ and $^1T_{2g}$ are split. Assuming cylindric ligands X and L, the symmetry of the MX_5L complex is C_{4v}, and the splitting of the two octahedral states may be expressed in terms of the relative values of the AOM parameters of the two ligands. With $\delta\Delta_{oct} = \Delta_{oct}(L) - \Delta_{oct}(X)$, $\delta e_\sigma = e_\sigma(L) - e_\sigma(X)$, and $\delta e_\pi = e_\pi(L) - e_\pi(X)$, $^1T_{1g}$ is split as follows:

$$^1T_{1g} \rightarrow A^1E \oplus {}^1A_2 \tag{3}$$

$$E_{(^1A_2 \leftarrow {}^1A_1)} = \Delta_{oct}(X) - C \tag{4}$$

$$E_{(A^1E \leftarrow {}^1A_1)} = \Delta_{oct}(X) - C + \left(\frac{1}{4}\right)\delta\Delta_{oct} = \Delta_{oct}(X) - C + \left(\frac{3}{4}\right)\delta e_\sigma - \delta e_\pi \tag{5}$$

whereas, for $^1T_{2g}$, the AOM expressions are

$$^1T_{2g} \rightarrow B^1E \oplus {}^1B_2 \tag{6}$$

$$E_{(^1B_2 \leftarrow {}^1A_1)} = \Delta_{oct}(X) + 16B - C + \delta e_\sigma \tag{7}$$

$$E_{(B^1E \leftarrow {}^1A_1)} = \Delta_{oct}(X) + 16B - C + \left(\frac{1}{4}\right)\delta e_\sigma - \delta e_\pi \tag{8}$$

dx.doi.org/10.1021/ic401704r | *Inorg. Chem.* 2013, 52, 10653−10663

As such, from the (experimental or calculated) energy values of the $^1T_{1g}$ components, the ligand-field strengths $\Delta_{oct}(X)$ and $\Delta_{oct}(L)$ may be obtained. Combined with this information, the energy splitting of $^1T_{2g}$ serves to obtain the values of δe_σ and δe_π.

Before applying the above equations to the CASPT2 results for $[Fe(CN)_5(py)]^{3-}$ to deduce the ligand-field parameters of X = cyanide and L = pyridine, two points should be noted. The first point concerns the value of Racah parameters B and C appearing in the above LF equations, and describing the difference in 3d interelectronic repulsion between the different LF states. For the parent $[Fe(CN)_6]^{4-}$ complex, values of B = 380 cm^{-1}, C = 2 800 cm^{-1} were obtained from the experimental LF spectrum.[35] The value of B is strongly reduced with respect to the free Fe(II) value of 1060 cm^{-1} ($\beta = B_{complex}/B_{ion}$ = 0.36), whereas the ratio C/B in the complex (7.37) is considerably larger than the free-ion value (4.41). The LF explanation of this strong "nephelauxetic" reduction of B and C is delocalization of the Fe 3d electron cloud on the ligands caused by covalent Fe−CN bonds. From the plots of the valence orbitals (Figure 2) and their composition (Table 2) in $[Fe(CN)_5(py)]^{3-}$, it is clear that the Fe−CN σ bonds are considerably more covalent than the Fe−CN π-bonds. Comparing the ligands cyanide and pyridine, we find no significant difference between the composition of the orbitals involving either Fe−CN σ-bonds or Fe−py σ-bonds. For this reason, we feel that we can safely use the values of the Racah parameters from the parent hexacyano complex to fit the LF spectrum of the pentacyano complex $[Fe(CN)_5(py)]^{3-}$ and the other $[Fe(CN)_5L]^{n-}$ complexes considered next.

The second point to note is that, for the pyridine ligand, we should have, in principle, defined two e_π parameters ($e_{\pi\|}$ and $e_{\pi\perp}$) rather than one e_π parameter, referring to the Fe−py π interactions parallel and perpendicular to the pyridine plane. However, the data in Table 4 indicate that the actual π-anisotropic character of pyridine is very limited. We find that the effective symmetry of the $[Fe(CN)_5(py)]^{3-}$ complex is close to C_{4v}, i.e., the states A^1B_2, A^1B_1 (corresponding to A^1E in C_{4v}) are split by only 103 cm^{-1}, whereas a larger but still limited splitting of 791 cm^{-1} is found for B^1B_2 and B^1B_1 (corresponding to B^1E in C_{4v}). This limited π-anisotropy of the pyridine ligand is an indication that Fe−py π-interactions are quite unimportant in the considered complex. This may be counterintuitive, given that the pyridine π^* orbitals are low-lying (i.e., giving rise to low-lying CT states; see the next section); therefore, it might be expected to considerably interact with the d_{xz} orbital, but not with the d_{yz} orbital. However, as can be seen from Figure 2 and Table 2, orbital interactions between Fe d_{xz} and the py π-orbitals of the same (b_1) symmetry are, in fact, quite limited. The d_{xz} orbital just shows a small lobe on the py N atom, whereas both py $\pi(b_1)$ and py $\pi^*(b_1)$ only contain 5% d_{xz} character.

Assuming C_{4v} symmetry, i.e., averaging the energy over the two ^1E components, and making use of the Racah parameters from the parent $[Fe(CN)_6]^{4-}$ complex, we may use the CASPT2(14,14) data from Table 4 (bs2 in water) to obtain the following ligand-field parameters: $\Delta_{oct}(CN)$ = 32 055 cm^{-1}, $\Delta_{oct}(py)$ = 11 517 cm^{-1}, δe_σ = −3944 cm^{-1}, δe_π = 1191 cm^{-1}. The ligand-field strength of ∼11 000 cm^{-1} for pyridine closely corresponds to previously reported data for this ligand, from analyses of the ligand-field spectra of the complexes Fe(py)$_4$(NCS)$_2$[49] and a series of ferrous trans-bis(pyridine)bis(β-diimine) complexes.[50] Moreover, the lower value obtained for $\Delta_{oct}(py)$ in comparison to $\Delta_{oct}(CN)$ correctly accounts for the lower ability of py to stabilize the complex as a whole. This fact is corroborated by the experimental evidence that $[Fe(CN)_5(py)]^{2-}$ has a lower reduction potential than $[Fe(CN)_6]^{3-}$, something that can be assigned to the less important π interaction between Fe(II) and py, in comparison to CN$^-$.[31]

Low-Lying LF States, as a Function of L. In this section, we present the results obtained from CASPT2(14,14) calculations on the four lowest LF states of $[Fe(CN)_5L]^{n-}$, as a function of the heterocyclic ligand L (cf Figure 1).[51] The results are shown in Table 5. For simplicity, all calculated states are labeled according to C_{2v} symmetry, even if, in some of the complexes (i.e., with L = pic, acpy, and mpz$^+$), the actual symmetry is only C_s. In order to obtain a consistent set of AOM parameters, we also decided to include a calculation of the LF spectrum of the parent octahedral $[Fe(CN)_6]^{4-}$ complex and the related $[Fe(CN)_5(NH_3)]^{3-}$ complex using the same CASPT2 approach (a CAS(10,10) space was used for both complexes, as they have no low-lying π^* orbitals). The calculated excitation energies for $[Fe(CN)_6]^{4-}$—30 626 cm^{-1} for $^1T_{1g} \leftarrow {}^1A_{1g}$ and 36 487 cm^{-1} for $^1T_{2g} \leftarrow {}^1A_{1g}$—closely correspond to the results obtained in our previous study[22] and are close (to within 1000 cm^{-1} of the experimental excitation energies: 31 000 and 37 040 cm^{-1}).[35] Consequently, the ligand-field strength $\Delta_{oct}(CN)$ obtained from the calculated spectrum of $[Fe(CN)_6]^{4-}$ (eq 1, 33 426 cm^{-1}) is also close to the value reported in the literature (33 800 cm^{-1}).[35] This confirms the accuracy of the present CASPT2 approach.

However, when looking at the data in Table 5 for the A $^1A_2$ state in the pentacyano complexes, corresponding to a ($d_{x^2-y^2} \rightarrow d_{xy}$) excitation in the equatorial plane, we find that the energy of this state is quite strongly dependent on the axial ligand L, dropping by 5 000 cm^{-1} when moving down in the table. This is obviously not in line with the AOM premise of ligand additivity, according to which the energy of this transition should depend only on $\Delta_{oct}(CN)$ (eq 4), and therefore remain constant for the different $[Fe(CN)_5L]^{n-}$ complexes. When comparing the value of the $\Delta_{oct}(CN)$ obtained from the $[Fe(CN)_6]^{4-}$ spectrum, 33 426 cm^{-1}, to the value obtained from the AOM analysis of the pyridine

Table 5. Excitation Energies of the Lowest LF States of $[Fe(CN)_5L]^{n-}$, as a Function of the Ligand L

	CASPT2 Excitation Energy (cm^{-1})					
	A^1B_2	A^1B_1	A^1A_2	A^1A_1	Relative AOM Parameters (cm^{-1})	
ligand, L	$d_{yz} \rightarrow d_{z^2}$	$d_{xz} \rightarrow d_{z^2}$	$d_{x^2-y^2} \rightarrow d_{xy}$	$d_{x^2-y^2} \rightarrow d_{z^2}$	$\delta\sigma'(L)^a$	$\delta\pi'(L)^b$
CN$^-$ [c]	30 626	30 626	30 626	36 487	6449	−1881
NH_3 [c]	23 910	23 906	29 881	30 038	0	0
pic [d]	24 021	24 315	29 403	29 860	−178	−394
py [d]	24 069	24 172	29 255	29 862	−176	−345
pz [d]	24 414	24 806	29 239	29 766	−272	−906
cnpy [d]	24 285	24 622	28 690	29 837	−201	−696
acpy [d]	24 296	24 596	27 235	30 010	−28	−561
mpz$^+$ [d]	25 214	25 614	25 262 [e]	30 507	469	−1154

[a] $\delta\sigma'(L) = e_\sigma(L) - e_\sigma(NH_3)$. [b] $\delta\pi'(L) = e_\pi(L) - e_\pi(NH_3)$. [c] CASPT2-(10,10) results in water, using bs2. [d] CASPT2(14,14) results in water, using bs2. [e] Calculated using average orbitals for the $A^1A_2(d_{x^2-y^2} \rightarrow d_{xy})$ LF and $b^1A_2(d_{x^2-y^2} \rightarrow \pi^*_{a_2})$ CT states, and containing significant CT character.

dx.doi.org/10.1021/ic401704r | Inorg. Chem. 2013, 52, 10653−10663

Table 6. Charge-Transfer (CT) States for $[Fe(CN)_5(py)]^{3-}$ under Vacuum and Water, Using Different Basis Sets

		CASPT2(14,14) Excitation Energy (cm^{-1})				Oscillator Strength
state	principal excitation[a]	vacuum,[b] bs2	water, bs1	water, bs2	water, bs3	water, bs2
a^1A_1	$d_{xz} \rightarrow \pi^*_{b_1}$	7 716	20 384	21 604	21 569	1.2×10^{-1}
a^1A_2	$d_{yz} \rightarrow \pi^*_{b_1}$	5 792	20 486	21 813	21 823	0.0
a^1B_1	$d_{x^2-y^2} \rightarrow \pi^*_{b_1}$	6 207	21 412	22 809	22 812	1.6×10^{-4}
b^1B_1	$d_{yz} \rightarrow \pi^*_{a_2}$	10 829	25 504	26 759	26 860	5.7×10^{-4}
b^1A_2	$d_{x^2-y^2} \rightarrow \pi^*_{a_2}$	10 972	25 555	26 868	26 914	0.0
a^1B_2	$d_{xz} \rightarrow \pi^*_{a_2}$	11 999	25 870	27 328	27 431	2.5×10^{-3}

[a]The ground-state configuration is X^1A_1 with configuration $(d_{xz})^2(d_{yz})^2(d_{x^2-y^2})^2(\pi^*_{b_1})^0(\pi^*_{a_2})^0$. [b]At ground-state geometry obtained in water.

Table 7. $^1A_1$ CT State for $[Fe(CN)_5(py)]^{3-}$ under Vacuum and Different Solvents Using Basis Set 2

			CASPT2		
solvent	acceptor number, AN[a]	dielectric constant, ε	energy (cm^{-1})	oscillator strength	experiment[c]
under vacuum			7 716	0.128	
in acetone	12.5	20.70	20 516	0.122	*b*
in acetonitrile	18.9	36.64	21 085	0.120	*b*
in DMSO	19.3	46.70	20 837	0.127	20 510
in ethanol	37.1	24.55	20 692	0.122	24 930
in ethanol (+5)[d]			22 402		
in methanol	41.3	32.63	21 079	0.119	25 180
in methanol (+5)[d]			22 720		
in water	54.8	78.39	21 604	0.118	27 320
in water (+5)[d]			23 139		
water (+14)[e]			29 453		

[a]From Mayer.[54] [b]Unknown. [c]Unless noted otherwise, data taken from ref 33. [d]Five explicit solvent molecules plus PCM. [e]Fourteen explicit water molecules plus PCM.

substituted complex in the previous section, 32 055 cm^{-1}, we see that the value of $\Delta_{oct}(CN)$ that comes out of the above AOM equations is indeed significantly dependent on the considered complex. The energy variations of the A $^1A_2$ state are caused by the presence of low-lying charge-transfer transitions to the $\pi^*_{a_2}$ orbital, mixing with the LF transitions into the d_{xy} orbital (of the same symmetry). In Table 5, the different ligands are ordered with respect to a decreasing A $^1A_2$ energy. We note already at this point that we will find the same ordering when presenting our results for the relative energy of the intense CT transition in the $[Fe(CN)_5L]^{n-}$ complexes as a function of L (Table 8). The lower the energy of the CT transitions to L π^* orbitals, the more they interfere with the LF transitions of the same symmetry, leading to the observed breakdown of the simple AOM equations.

In order to circumvent the problems with the A^1A_2 state and still obtain a reasonable set of ligand-field parameters for the different *N*-heterocyclic ligands L, we therefore decided to base our ligand-field analysis only on the three other states, corresponding to a LF transition into d_{z^2}, A^1A_1, A^1B_1, A^1B_2 (averaging the energy of the latter two $^1E(C_{4v})$ components), and to use the spectrum of the $[Fe(CN)_5(NH_3)]^{3-}$ complex as a reference.[52,53] Only relative values of the AOM parameters of the different L with respect to NH_3 are given in Table 5. However, as we may conveniently assume that $e_\pi(NH_3) = 0$, the values of $\delta\pi'(L)$ may also be interpreted as absolute $e_\pi(L)$ values. Our observation is that all N-donor ligands are much weaker σ donors than CN^-, while, among themselves, they are all slightly weaker than NH_3, with exception of mpz^+, with a positive $\delta\sigma'$ value of 469 cm^{-1}. All *N*-heterocyclic ligands also act as weak π-acceptors, weaker than CN^-, with mpz^+ also showing the strongest π-accepting properties. Note also that, even for the latter ligand, the energy difference between the two states A^1B_1 and A^1B_2 amounts to only 400 cm^{-1}, thus reflecting a limited π-anisotropy. A similar or even smaller energy difference is found for the other ligands.

We finally note that, for L = mpz^+, a LF band has been reported experimentally in water[32] at $\tilde{\nu}$ = 26 300 cm^{-1}, close to the two symmetry-allowed LF transitions in Table 5. For the other L, the LF transitions are masked by the intense CT band, studied in the next section. As we shall see further (Table 8 and Figure 4), this CT is strongly red-shifted in the case of L = mpz^+, thus leaving room for a weak LF transition in the 26 000 cm^{-1} region.

Charge-Transfer Spectra. *CT Spectrum of $[Fe(CN)_5(py)]^{3-}$.* Since preliminary CASSCF studies indicated that excitations to the pyridine π^* orbital with the highest energy (b_1 symmetry) are very high-lying (in the UV region), we report here only the results calculated for the six lowest CT states of $[Fe(CN)_5(py)]^{3-}$, originating from the Fe $3d_\pi$ orbitals into the lowest two pyridine π^* orbitals (b_1 and a_2). Calculations were performed both under vacuum and in aqueous solution. The results are presented in Table 6.

A comparison of the results obtained with the three basis sets leads to the same conclusion as already found for the LF states (Table 4), i.e., that a significant improvement of the results are obtained when going from bs1 to bs2, but not from bs2 to bs3. As the calculations with bs3 involve a much higher computational effort than with bs2, we have chosen to use bs2 in all subsequent calculations (cf Table 1).

The solvent effect on the CT energies is remarkable: differences ranging between 13 800 and 16 600 cm^{-1} are

dx.doi.org/10.1021/ic401704r | Inorg. Chem. 2013, 52, 10653−10663

observed between the calculated excitation energies under vacuum and in water. All states are strongly stabilized by the inclusion of the solvent but the effect is more pronounced for the ground state. As a consequence, relative energies in water are larger than those observed under vacuum.

Even though all excitations in Table 6 are of CT type, only one transition has considerable oscillator strength. This is consistent with the appearance of just one strong band in the experimental spectrum of $[Fe(CN)_5(py)]^{3-}$ in water.[33] The band concerned involves the excitation of an electron from the Fe $3d_\pi$ orbital that is oriented perpendicular to the aromatic ring of the pyridine ligand ($3d_{xz}$) into a pyridine π^* orbital of the same symmetry (b_1). Since both orbitals have the same symmetry, they may overlap. However, as indicated by the numbers in Table 2, the actual mixing between the $3d_{xz}$ and py $\pi^*_{b_1}$ in the bonding and antibonding b_1 combination is quite limited, indicating only weak overlap. As will be further discussed in the next section, the $a^1A_1 \leftarrow X^1A_1$ excitation rather gains intensity from configuration interaction between both states rather than from mixing at the MO level.

The energy obtained from CASPT2(14,14) for the $a^1A_1 \rightarrow X^1A_1$ excitation in water, however, is only 21 604 cm^{-1}. This is lower, by as much as 5700 cm^{-1} than the experimentally reported band maximum of 27 320 cm^{-1} in the spectrum of aqueous $[Fe(CN)_5(py)]^{3-}$.[33] To further investigate the origin of this large discrepancy, we decided to calculate the intense $a^1A_1 \rightarrow X^1A_1$ excitation in the $[Fe(CN)_5(py)]^{3-}$ spectrum in a series of different solvents. The results of these calculations are shown in Table 7. The solvents considered may be subdivided into two categories: aprotic solvents (e.g., acetone, acetonitrile, and DMSO) and protic solvents (e.g., methanol, ethanol, and water). Two properties of the solvents may potentially play a role in the excitation energy of the CT transition in these negatively charged complexes: the dielectric constant (ε) and Lewis acidity. The strength of the solvent as a Lewis acid has been quantified (based on the ^{31}P nuclear magnetic resonance (^{31}P NMR) chemical shift of triethylphosphine) by the so-called acceptor number (AN) of the solvent.[54] Both ε and AN are given for the different solvents in Table 7. One can see that the aprotic solvents indeed systematically show a lower AN than the protic solvents, whereas, in the latter group, the AN increases with Lewis acidity: ethanol < methanol < water. Since the dielectric PCM model used in this work considers the solvent medium as a simple polarizable dielectric, a priori, it cannot be expected to fully cope with Lewis acidity, and this might be the origin of the failure of PCM to model the effect of the aqueous environment on the CT spectrum of $[Fe(CN)_5(py)]^{3-}$. As Table 7 indicates, the actual value of ε does not considerably affect the calculated energy of the CT transitions: although the inclusion of a solvent causes a huge shift upward, variations between the different solvents are modest (at most, 1100 cm^{-1}). The general trend is that the transition energy increases with ε, although there are some small fluctuations (e.g., acetonitrile giving a higher transition energy than DMSO).

Unfortunately, no experimental data are available for acetone and acetonitrile. Taking DMSO as a representative, we note that the effect of an aprotic solvent seems to be reproduced very well by the PCM model. Indeed, the CASPT2 excitation energy in DMSO agrees to within 400 cm^{-1} with the experimental value. In contrast, for the protic solvents, the PCM model (alone) obviously cannot capture the solvent effect to its full extent. The calculated excitation energy in all three solvents is considerably lower than the experiment. For ethanol and methanol, the difference is ~4000 cm^{-1}, and one can see that the relative value between both solvents is correctly reproduced. However, for water, the deviation from experiment further increases to 5700 cm^{-1}. In an attempt to reduce this difference, we have performed additional calculations on $[Fe(CN)_5(py)]^{3-}$ in these three solvents, in which, now, many solvent molecules are treated explicitly in the quantum model. We started by placing five solvent molecules in the vicinity of the five CN ligands. As depicted in Figure 3, each of

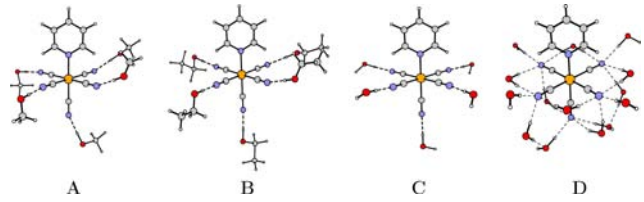

Figure 3. PBE0/def2-QZVPP(Fe)/def2-TZVP(other atoms) geometry for $[Fe(CN)_5(py)]^{3-}$, using either 5 explicit solvent molecules ((A) methanol, (B) ethanol, and (C) water) and COSMO, or (D) 14 explicit water molecules and COSMO.

the solvent molecules forms a hydrogen bond with one of the CN ligands. Solvation of the supramolecular aggregate was considered by the PCM model. After reoptimizing the structure with PBE0, the intense band in the spectrum was recalculated with CASPT2. A shift upward by ~1500−1800 cm^{-1} was obtained. However, the remaining deviation from the experiment is still significant: ~2500 cm^{-1} for methanol and ethanol, and >4000 cm^{-1} for water. For the latter solvent, supramolecular aggregates with extra water molecules were constructed, using different numbers and starting positions for the explicit H_2O. Up to 14 explicit water molecules were found to bind to the complex by means of hydrogen bonds, as shown in Figure 3. The calculated excitation energy for this complex, 29 453 cm^{-1}, is now too high, compared to the experimental band position. Obviously, the static picture provided by the DFT geometry optimizations now leads to an overestimation of the total number of water molecules that, in reality, will simultaneously hydrogen-bind to the complex, and a more realistic number might be provided by molecular dynamics (MD) simulations. However, such calculations are outside the scope of the present study. Still, the conclusion from the present exercise is that underestimation of the transition energy should be traced back to the failure of the PCM model, rather than to possible errors in the CASPT2 treatment. Improved solvent models, such as the direct-COSMO-RS model,[16,55] should be able to provide a more accurate description of the effect of hydrogen bonding on CT energies in protic solvents. However, these models are not available in combination with the CASPT2 method.

Charge-Transfer Spectra of Complexes with Different L. The role played by ligand L in $[Fe(CN)_5L]^{n-}$ on the excitation energy and oscillator strength of the intense CT band was investigated by performing CASPT2(14,14) calculations in DMSO[56] for the following ligands L (cf. Figure 1): pyridine (py), 4-methyl-pyridine (pic), 4-cyano-pyridine (cnpy), 4-acetyl-pyridine (acpy), pyrazine (pz), and the *N*-methylpirazinium ion (mpz^+). The results are shown in Table 8 and Figure 4. As was already noted above for $[Fe(CN)_5(py)]^{3-}$ in DMSO, all calculated excitation energies are in close

dx.doi.org/10.1021/ic401704r | *Inorg. Chem.* 2013, 52, 10653−10663

Table 8. Energy, Character, and Intensity of the a^1A_1 Charge-Transfer (CT) State in Different $[Fe(CN)_5L]^{n-}$ in DMSO[a]

ligand, L	CASPT2(14,14) energy (cm^{-1})	oscillator strength	transition dipole moment, μ(a.u.)	mix (%)[b]	experimental[33] energy (cm^{-1})
pic	21 992	0.13	1.41	8.6	21 880
py	20 837	0.13	1.42	8.6	20 510
pz	16 641	0.16	1.76	13.4	16 920
cnpy	14 330	0.18	2.06	14.9	15 380
acpy	13 498	0.18	2.09	15.2	13 790
mpz^+	10 249	0.25	2.82	28.9	c

[a]Calculations performed with basis set 2. [b]Percentage mixing of $(d_{xz})^2(d_{yz})^2(d_{x^2-y^2})^2$ character in the wave function of the a^1A_1 state. [c]Unknown.

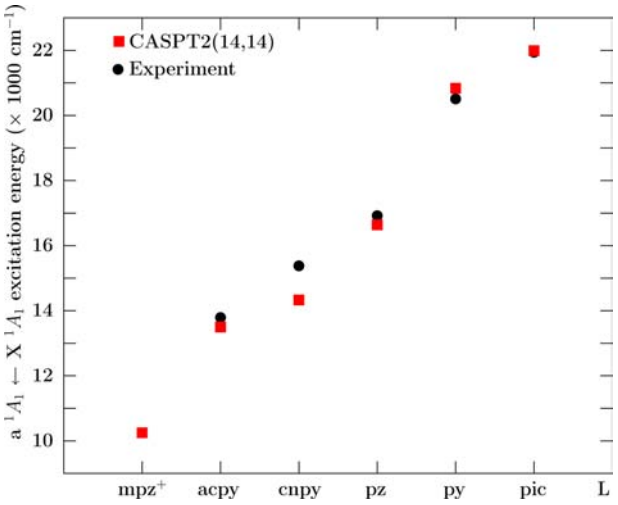

Figure 4. Comparison between theoretical and experimental CT excitation energy for $[Fe(CN)_5L]^{n-}$ in DMSO.

correspondence to the experiment, with a maximum deviation of 1000 cm^{-1} for L = cnpy. The CT band position is red-shifted in the order L = pic > py > pz > cnpy > acpy > mpz^+, indicating a decreasing energy separation between the Fe $3d_{xz}$ and the L π^*-orbitals in the same order. For L = mpz^+, no experimental information concerning the intense CT excitation is available. Our calculations predict that this excitation occurs at a very low energy, i.e., in the near-infrared (NIR) region (10 249 cm^{-1}). Experimental data for the oscillator strengths in DMSO have not been reported. However, in water, it was found that the extinction coefficient of the intense CT band increases as its transition energy decreases.[31] Such a trend is not self-evident, given the following relation between the oscillator strength (f), transition energy (ΔE), and transition dipole moment (μ) of an electronic transition:

$$f = \frac{2}{3}\Delta E|\mu|^2 \qquad (10)$$

In ref 31, the increasing band intensity with decreasing energy was attributed to an increasing degree of Fe 3d–L π^* interaction when moving down in the series of L included in Table 8. As can be seen from this table, the experimental trend is confirmed by our calculations, and this trend may be ascribed to a strongly increasing transition dipole moment between the X^1A_1 ground state and the $a^1A_1(d_{xz} \rightarrow \pi^*_{b_1})$ CT state, as the energy separation between the two orbitals involved decreases. According to our calculations, however, the increase of μ cannot solely be attributed to an increasing covalent interaction between these two orbitals. From a Mulliken population analysis (cf. Table 2), we find that the contribution of L π^* character in the bonding b_1 orbital and vice versa remains constant, at ~5% for all L, except mpz^+, for which it increases to 11%. However, we also find that the decreasing energy difference between the two states involved in the CT excitation gives rise to an increasing interconfigurational mixing between these two states. In particular, we observe a considerably increasing contribution of $(d_{xz})^2(d_{yz})^2(d_{x^2-y^2})^2$ character in the CASSCF wave function of the excited state a^1A_1. This contribution is also included in Table 8. It was obtained by rewriting the CASSCF(14,14) wave function of the a^1A_1 state, in terms of localized orbitals[57] obtained from a (Cholesky) localization procedure[58] of the two b_1 orbitals involved in the CT excitation. This way, the contribution from the "pure" $(d_{xz})^2$ configuration may be obtained. As can be seen, this contribution increases from <9% for L = py and pic to ~30% for L = mpz^+. Given this observation, it should be clear that the use of multiconfigurational methods such as CASPT2 is indispensable for a balanced and reliable description of the electronic spectra of the present $[Fe(CN)_5L]^{n-}$ complexes.

CONCLUSIONS

In this paper, we have provided a detailed computational study of the structures and electronic spectra of complexes of formula $[Fe(CN)_5L]^{n-}$, in which L is an *N*-heterocyclic ligand (Figure 1), with particular emphasis on the description of solvent effects. A comparison of the (DFT) structure of $[Fe(CN)_5py]^{3-}$ in the gas phase and different solvents indicated that implicit solvation effects should be included in the calculations to obtain accurate bond distances and avoid tilting of the cyanides, but the precise choice of the solvent (dielectric constant) is not important.

A detailed study of the ligand-field spectrum of $[Fe(CN)_5(py)]^{3-}$ was performed, including a ligand-field analysis, based on the standard angular overlap model (AOM) equations for a monosubstituted octahedral d^6 complex, and making use of the Racah parameters of the parent $[Fe(CN)_6]^{4-}$ complex. From a comparison with the closely related $[Fe(CN)_5(NH_3)]^{3-}$ complex, relative values of the AOM e_σ and e_π parameters of the different ligands L could be deduced. From this analysis, we found that all *N*-heterocyclic ligands are weak π-acceptors, with an e_π value ranging between −345 cm^{-1} (py) and −1154 cm^{-1} (mpz^+). The latter ligand was also found to be the strongest σ-donor, with all other ligands L being slightly weaker σ-donors than NH_3. However, our calculations also indicated that the presence of low-lying charge-transfer (CT) states in the spectra leads to a breakdown of the AOM premise of ligand additivity in the prediction of the position of the LF bands.

For the LF excited states, excitation energies obtained from CASPT2 show little variation between being under vacuum and being in water. Based on the calculated oscillator strengths is also possible to predict that only one LF band may possibly be observed in the experimental spectrum of $[Fe(CN)_5py]^{3-}$,

dx.doi.org/10.1021/ic401704r | Inorg. Chem. 2013, 52, 10653−10663

composed of two nearly degenerate transitions to $AB_1(d_{xz} \rightarrow d_{z2})$ and AB_2 $(d_{yz} \rightarrow d_{z2})$ states. For all ligands except mpz^+, this LF band falls in the region of the much more intense CT transition; therefore, this is not observed in the experiment. For L = mpz^+, the CT band is strongly red-shifted, such that the LF band, calculated at ~25 400 cm^{-1}, is also observed experimentally in water (at 26 300 cm^{-1}).

As observed experimentally, the CT spectrum of the different $[Fe(CN)_5L]^{n-}$ complexes is predicted to consist of only one intense band, corresponding to a transition from d_{xz} to the *N*-heterocyclic $\pi^*_{b_1}$ orbital. As opposed to the LF states, and conforming with the experiment, the transition energy of this CT is extremely sensitive to the solvent. The PCM method is able to partially account for the solvent effect. In the case of DMSO (and, presumably, other aprotic solvents) the resulting CASPT2 excitation energy is in excellent agreement (within 400 cm^{-1}) with the experimental band position. However, in the case of the protic solvents (water, ethanol, and methanol), the CASPT2 excitation energies in a PCM environment are too low, by up to 5700 cm^{-1}. These solvents may interact with the cyanide ligands through hydrogen bonding, and calculations including five explicit solvent molecules (each binding to one CN) were shown to provide a significant improvement of the transition energy, although the difference with experiment is still more than 4000 cm^{-1} for water. For the latter solvent, a structure with as many as 14 explicit water molecules was optimized, and was used to prove that water molecules in the second and higher coordination sphere indeed assist in raising the energy of the CT transition by several thousand wavenumbers.

As for the comparison between different ligands, our CASPT2 calculations nicely reproduce both the observed order in excitation energies in DMSO,

$$pic > py > pz > cnpy > acpy > (mpz)^+$$

and the concomitant increase in intensity of the CT band. The latter may be ascribed to an increasing mixing between the ground-state configuration and the excited-state configuration as the energy difference between the two states decreases.

Overall, we have shown that the present CASPT2 approach is capable of predicting the electronic spectra of the studied $[Fe(CN)_5L]^{n-}$ complexes with good accuracy (that is, to within 1000 cm^{-1} of the experimentally observed band positions).

AUTHOR INFORMATION

Corresponding Author

*E-mail addresses: formiga@iqm.unicamp.br (A.L.B.F.), kristin.pierloot@chem.kuleuven.be (K.P.).

Notes

The authors declare no competing financial interest.

ACKNOWLEDGMENTS

This research has been supported by grants from the Flemish Science Foundation (FWO) and from the Concerted Research Action of the Flemish Government (GOA). A.L.B.F. would like to thank São Paulo State Research Foundation (FAPESP) for a research grant (No. 2010-15762-5) to visit KU Leuven and Conselho Nacional de Desenvolvimento Cientfico e Tecnológico (CNPq) for financial support (Grant Nos. 479415/2009-9 and 402627/2012-1).

REFERENCES

(1) (a) Wang, S.; Ding, X.-H.; Li, Y.-H.; Huang, W. *Coord. Chem. Rev.* **2012**, *256*, 439−464. (b) Wang, S.; Ding, X.-H.; Zuo, J.-L.; You, X.-Z.; Huang, W. *Coord. Chem. Rev.* **2011**, *255*, 1713−1732. (c) Atanasov, M.; Comba, P.; Hausberg, S.; Martin, B. *Coord. Chem. Rev.* **2009**, *253*, 2306−2314. (d) Jannuzzi, S. A. V.; Martins, B.; Felisberti, M. I.; Formiga, A. L. B. *J. Phys. Chem. B* **2012**, *116*, 14933−14942.

(2) (a) Ferlay, S.; Mallah, T.; Ouahès, R.; Veillet, P.; Verdaguer, M. *Nature* **1995**, *378*, 701−703. (b) Verdaguer, M.; Bleuzen, A.; Marvaud, V.; Vaissermann, J.; Seuleiman, M.; Desplanches, C.; Scuiller, A.; Train, C.; Garde, R.; Gelly, G.; Lomenech, C.; Rosenman, I.; Veillet, P.; Cartier, C.; Villain, F. *Coord. Chem. Rev.* **1999**, *190−192*, 1023−1047. (c) Holmes, S. M.; Girolami, G. S. *J. Am. Chem. Soc.* **1999**, *121*, 5593−5594.

(3) Zadrozny, J. M.; Freedman, D. E.; Jenkins, D. M.; Harris, T. D.; Iavarone, A. T.; Mathonière, C.; Clérac, R.; Long, J. R. *Inorg. Chem.* **2010**, *49*, 8886−8896.

(4) Endicott, J. F.; Chen, Y.-J. *Coord. Chem. Rev.* **2013**, *257*, 1676−1698.

(5) Baraldo, L. M.; Forlano, P.; Parise, A. R.; Slep, L. D.; Olabe, J. A. *Coord. Chem. Rev.* **2001**, *219−221*, 881−921.

(6) (a) Van den Heuvel, W.; Hendrickx, M. F. A.; Ceulemans, A. *Inorg. Chem.* **2007**, *46*, 8032−8037. (b) Clima, S.; Hendrickx, M. F. A. *Chem. Phys. Lett.* **2005**, *411*, 121−127. (c) Hendrickx, M. F. A.; Mironov, V. S.; Chibotaru, L. F.; Ceulemans, A. *Inorg. Chem.* **2004**, *43*, 3142−3150. (d) Hendrickx, M. F. A.; Chibotaru, L. F.; Ceulemans, A. *Inorg. Chem.* **2003**, *42*, 590−597. (e) Hendrickx, M. F. A.; Mironov, V. S.; Chibotaru, L. F.; Ceulemans, A. *J. Am. Chem. Soc.* **2003**, *125*, 3694−3695.

(7) Ene, C. D.; Lungu, A.; Mihailciuc, C.; Hillebrand, M.; Ruiz-Pérez, C.; Andruh, M. *Polyhedron* **2012**, *31*, 539−547.

(8) Roos, B. O.; Andersson, K.; Fülscher, M. P.; Malmqvist, P.-Å.; Serrano-Andrés, L.; Pierloot, K.; Merchán, M. In *Advances in Chemical Physics: New Methods in Computational Quantum Mechanics, Vol. XCIII*; Prigogine, I., Rice, S. A., Eds.; John Wiley & Sons: New York, 1996; pp 219−332.

(9) Pierloot, K. In *Computational Photochemistry, 16*; Olivucci, M., Ed.; Elsevier: Amsterdam, 2005; pp 279−315.

(10) Neese, F.; Petrenko, T.; Ganyushin, D.; Olbrich, G. *Coord. Chem. Rev.* **2007**, *251*, 288−327.

(11) González, L.; Escudero, D.; Serrano-Andrés, L. *ChemPhysChem* **2012**, *13*, 28−51.

(12) (a) Becke, A. D. *J. Chem. Phys.* **1993**, *98*, 5648−5652. (b) Lee, C.; Yang, W.; Parr, R. G. *Phys. Rev. B* **1988**, *37*, 785−789.

(13) Adamo, C.; Barone, V. *J. Chem. Phys.* **1999**, *110*, 6158−6169.

(14) (a) Weigend, F.; Häser, M.; Patzelt, H.; Ahlrichs, R. *Chem. Phys. Lett.* **1998**, *294*, 143−152. (b) Weigend, F.; Furche, F.; Ahlrichs, R. *J. Chem. Phys.* **2003**, *119*, 12753−12762.

(15) (a) Ahlrichs, R.; Bär, M.; Häser, M.; Horn, H.; Kölmel, C. *Chem. Phys. Lett.* **1989**, *162*, 165−169. (b) Treutler, O.; Ahlrichs, R. *J. Chem. Phys.* **1995**, *102*, 346.

(16) Klamt, A. *J. Phys. Chem.* **1995**, *99*, 2224−2235.

(17) Karlström, G.; Lindh, R.; Malmqvist, P.-Å.; Roos, B. O.; Ryde, U.; Veryazov, V.; Widmark, P.-O.; Cossi, M.; Schimmelpfennig, B.; Neogrady, P.; Seijo, L. *Comput. Mater. Sci.* **2003**, *28*, 222−239.

(18) Aquilante, F.; De Vico, L.; Ferré, N.; Ghigo, G.; Malmqvist, P.-Å.; Neogrády, P.; Pedersen, T. B.; Pitoňák, M.; Reiher, M.; Roos, B. O.; Serrano-Andrés, L.; Urban, M.; Veryazov, V.; Lindh, R. *J. Comput. Chem.* **2010**, *31*, 224−247.

(19) (a) Roos, B. O.; Lindh, R.; Malmqvist, P.-Å.; Veryazov, V.; Widmark, P.-O. *J. Phys. Chem. A* **2004**, *108*, 2851−2858. (b) Roos, B. O.; Lindh, R.; Malmqvist, P.-Å.; Veryazov, V.; Widmark, P.-O. *J. Phys. Chem. A* **2005**, *109*, 6575−6579.

(20) The exact role of the Cholesky decomposition threshold is not directly related to a total energy threshold, but to the accuracy of the individual integral approximations. A more-detailed investigation of what this means for the total accuracy with CASSCF/CASPT2 can be found in: Boström, J.; Delcey, M. G.; Aquilante, F.; Serrano-Andrés, L.; Pedersen, T. B.; Lindh, R. *J. Chem. Theory Comput.* **2010**, *6*, 747−754.

(21) Aquilante, F.; Malmqvist, P.-Å.; Pedersen, T. B.; Ghosh, A.; Roos, B. O. *J. Chem. Theory Comput.* **2008**, *4*, 694−702.
(22) Pierloot, K.; Vanpraet, E.; Vanquickenborne, L. G.; Roos, B. O. *J. Phys. Chem.* **1993**, *97*, 12220−12228.
(23) Vancoillie, S.; Zhao, H.; Tran, V. T.; Hendrickx, M. F. A.; Pierloot, K. *J. Chem. Theory Comput.* **2011**, *7*, 3961−3977.
(24) Pierloot, K.; Zhao, H.; Vancoillie, S. *Inorg. Chem.* **2010**, *49*, 10316−10329.
(25) Radoń, M.; Broclawik, E.; Pierloot, K. *J. Chem. Theory Comput.* **2011**, *7*, 898−908.
(26) Chen, H.; Song, J.; Lai, W.; Wu, W.; Shaik, S. *J. Chem. Theory Comput.* **2010**, *6*, 940−953.
(27) Domingo, A.; Angels Carvajal, M.; de Graaf, C.; Sivalingam, K.; Neese, F.; Angeli, C. *Theor. Chem. Acc.* **2012**, *131*, 1264.
(28) Malmqvist, P.-Å.; Roos, B. O. *Chem. Phys. Lett.* **1989**, *155*, 189−194.
(29) Miertuš, S.; Scrocco, E.; Tomasi, J. *Chem. Phys.* **1981**, *55*, 117−29.
(30) (a) Tullberg, A.; Vannerberg, N.-G. *Acta Chem. Scand.* **1974**, *28A*, 551−562. (b) Taylor, J. C.; Mueller, M. H.; Hitterman, R. L. *Acta Crystallogr., Sect. A: Cryst. Phys., Diffr., Theor. Gen. Crystallogr.* **1970**, *A26*, 559−567.
(31) Toma, H. E.; Malin, J. M. *Inorg. Chem.* **1973**, *12*, 1039−1045.
(32) Toma, H. E.; Giesbrecht, E.; Malin, J. M.; Fluck, E. *Inorg. Chim. Acta* **1975**, *14*, 11−15.
(33) Toma, H. E.; Takasugi, M. S. *J. Solution Chem.* **1983**, *12*, 547−561.
(34) Pierloot, K.; van Besien, E. *J. Chem. Phys.* **2005**, *123*, 204309.
(35) Alexander, J. J.; Gray, H. B. *J. Am. Chem. Soc.* **1968**, *90*, 4260−4271.
(36) Malin, J. M.; Schmidt, C. F.; Toma, H. E. *Inorg. Chem.* **1975**, *14*, 2924−2928.
(37) Lever, A. B. P. *Inorganic Electronic Spectroscopy*; Elsevier: Amsterdam, 1984.
(38) Lever, A. B. P.; Solomon, E. I. In *Inorganic Electronic Structure and Spectroscopy, Vol. I*; Solomon, E. I., Lever, A. B. P., Eds.; John Wiley & Sons: New York, 1999; pp 1−92.
(39) Schäffer, C. E.; Jørgensen, C. K. *Mol. Phys.* **1965**, *9*, 401.
(40) Pierloot, K. In *Computational Organometallic Chemistry*; Cundari, T. R., Ed.; Marcel Dekker: New York, 2001; pp 123−158.
(41) Pierloot, K. *Mol. Phys.* **2003**, *101*, 2083−2094.
(42) Anthon, C.; Bendix, J.; Schäffer, C. E. *Inorg. Chem.* **2004**, *43*, 7882−7886.
(43) Fouqueau, A.; Casida, M. E.; Lawson Daku, L. M.; Hauser, A.; Neese, F. *J. Chem. Phys.* **2005**, *122*, 044110.
(44) Ishii, T.; Tsuboi, S.; Sakane, G.; Yamashitac, M.; Breedlove, B. K. *Dalton Trans.* **2009**, 680−687.
(45) Schäffer, C. E.; Anthon, C.; Bendix, J. *Coord. Chem. Rev.* **2009**, *253*, 575−593.
(46) Atanasov, M.; Ganyushin, D.; Sivalingam, K.; Neese, F. *Struct. Bonding (Berlin)* **2012**, *143*, 149−220.
(47) Deeth, R. J.; Anastasi, A.; Diedrich, C.; Randell, K. *Coord. Chem. Rev.* **2009**, *253*, 795−816.
(48) Deeth, R. J. *Adv. Inorg. Chem.* **2010**, *62*, 1−39.
(49) Gerloch, M.; Woolley, R. G. *Prog. Inorg. Chem.* **1983**, *31*, 371−446.
(50) Riley, D. P.; Stone, J. A.; Busch, D. H. *J. Am. Chem. Soc.* **1977**, *99*, 767−777.
(51) Calculations on the two highest-lying LF states corresponding to an excitation from ($3d_{xz}$, $3d_{yz}$) to $3d_{xy}$ were also attempted, but mixing and root-flipping with low-lying CT states lead to lack of convergence for those L (cnpy, acpy, mpz^{+}) that have lower-lying π^* orbitals than py (cf. Table 8).
(52) A crystal field analysis of the experimental LF spectra of monosubstituted pentacyanoferrate complexes with different N-donor ligands (amino acids and related ligands) were already reported many years ago.[53] This study indicated that the ligand-field strength of such ligands is very close to that of NH_3. This conclusion is confirmed by the data in Table 5. However, the value of $\Delta_{oct}(NH_3)$ reported in the same paper, 23 300 cm^{-1}, is much larger than the presently reported value of Δ_{oct}(py). This is because, in ref 53, the relationship between *Dt* (describing the tetragonal perturbation in crystal field theory) and $\delta\Delta_{oct}$ was "scaled" to $Dt = 0{:}0628\delta\Delta_{oct}$, rather than using the standard relationship $Dt = {}^{1}/_{35}\delta\Delta_{oct}$. The reason for this scaling is not mentioned in the paper.
(53) Toma, H. E.; Batista, A. A.; Gray, H. B. *J. Am. Chem. Soc.* **1982**, *104*, 7509−7515.
(54) Mayer, U. *Pure Appl. Chem.* **1979**, *51*, 1697−1712.
(55) Renz, M.; Kess, M.; Diedenhofen, M.; Klamt, A.; Kaupp, M. *J. Chem. Theory Comput.* **2012**, *8*, 4189−4203.
(56) (a) DMSO is a strongly coordinating ligand and can substitute N-heterocycles in pentacyanoferrate(II) complexes very easily, making the experimental evaluation of these data very difficult. (b) Toma, H. E.; Malin, J. M.; Giesbrecht, E. *Inorg. Chem.* **1973**, *12*, 2084−2089.
(57) A CASSCF wave function is not unique in the sense that it is invariant (i.e., keeps its overall form and energy) under any unitary transformation of two or more of its active molecular orbitals, with concomitant transformation of the appropriate CI coefficients.
(58) Aquilante, F.; Pedersen, T. B.; Ade Merás, A. S.; Koch, H. *J. Chem. Phys.* **2006**, *125*, 174101.